Nuclear Engineering and Technology 54 (2022) 1541–1548

Contents lists available at ScienceDirect

Nuclear Engineering and Technology

journal homepage: www.elsevier.com/locate/net

Original Article

Effective thermal conductivity model of porous polycrystalline UO_2: A computational approach

Bohyun Yoon, Kunok Chang*

Department of Nuclear Engineering, Kyung Hee University, Yongin-City, South Korea

ARTICLE INFO

Article history:
Received 10 May 2021
Received in revised form
14 October 2021
Accepted 27 October 2021
Available online 30 October 2021

Keywords:
UO_2
Effective thermal conductivity
Computer simulation

ABSTRACT

The thermal conductivity of uranium oxide (UO_2) containing pores and grain boundaries is investigated using continuum-level simulations based on the finite-difference method in two and three dimensions. Steady-state heat conduction is solved on microstructures generated from the phase-field model of the porous polycrystal to calculate the effective thermal conductivity of the domain. The effects of porosity, pore size, and grain size on the effective thermal conductivity of UO_2 are quantified. Using simulation results, a new empirical model is developed to predict the effective thermal conductivity of porous polycrystalline UO_2 fuel as a function of porosity and grain size.

1. Introduction

Uranium dioxide (UO_2) is a primary fuel for nuclear power reactors for the past 60 years. Because the thermophysical property of nuclear fuel is critical for ensuring reactor safety and efficiency, regulation codes have been established for securing fuel performance, such as FRAPCON [1], which can predict the thermal properties of UO_2 during reactor operation. The material-property correlations in FRAPCON are based on extensive databases that have been accumulated over decades, and its predicted values are generally consistent with experimental values [1]. However, an empirical model cannot provide the property values for systems outside the experience range. Therefore, significant effort has been expanded to understand the effects of various features of irradiated UO_2 on its thermophysical properties and to develop more generally applicable models based on computational methods [2,3]. Atomistic [4–6] and continuum [7–9] simulations have been performed to predict the effects of grain boundaries and porosity on the thermal conductivity of porous polycrystals in several studies.

However, these studies were limited to two-dimensional (2D) or simple three-dimensional (3D) bicrystal systems. In a previous study [10], steady-state heat conduction analysis of a porous single crystal of UO_2 at the continuum level was performed, and it was discovered that conductivity was significantly affected by pore size, which was not considered in previous widely used physical models [5,11–13].

We developed a thermal conduction simulation code based on the finite difference method by implementing a CUDA-accelerated parallel computing skill, which enabled us to perform a 3D large-scale simulation in a previous study [10]. In this study, we expanded the microstructure to a polycrystal system to more adequately describe actual UO_2 fuel pellets. We performed a thermal analysis of the porous polycrystalline microstructure to investigate the effects of grain boundaries and pores on the effective conductivity of UO_2 in 2D and 3D systems, as well as proposed a simulation-based empirical model that can provide important guidelines for the effective thermal conductivity of high burn-up UO_2.

2. Methodology and numerical approach

2.1. Phase field model for grain growth with pores

We employed a phase-field model to generate polycrystalline microstructures of UO_2 fuels with pores [14]. The set of non-conserved order parameters indicates the grain orientations present in the matrix phase of the polycrystalline materials.

$$\eta_1(\boldsymbol{r},t),\ \eta_2(\boldsymbol{r},t),\ \cdots,\ \eta_P(\boldsymbol{r},t), \tag{1}$$

* Corresponding author.
E-mail address: kunok.chang@khu.ac.kr (K. Chang).

https://doi.org/10.1016/j.net.2021.10.040

$$\frac{\partial \eta_i(\boldsymbol{r},t)}{\partial t} = -L_i \frac{\delta F}{\delta \eta_i(\boldsymbol{r},t)},\ i=1,\ 2,\ \cdots,\ P, \tag{2}$$

where η_i $(i=1,\ 2,\ \cdots,\ P)$ is a nonconserved order parameter represented by position $(\boldsymbol{r})$ and time (t), and its evolution is obtained by solving the time-dependent Ginzburg–Landau equation shown in Eq. (2). We evolved only the active parameter (nonzero) [15] for computational efficiency.

The total free energy function F of a heterogeneous system of grains and pores is described as follows [16]:

$$F = \int_V \left[m\left(\sum_i^P \left(\frac{\eta_i^4}{4} - \frac{\eta_i^2}{2} \right) + \sum_i^P \sum_{j\neq i}^P \eta_i^2 \eta_j^2 \right) + \varepsilon \Phi \sum_{i=1}^P \eta_i^2 + \frac{\kappa_i}{2} \sum_i^P (\nabla \eta_i)^2 \right] dV. \tag{3}$$

where the free energy F has unit of J.

Using Eqs. (3) and (2), we obtain

$$\frac{\partial \eta_i(\boldsymbol{r},t)}{\partial t} = -L_i \left(m\left(-\eta_i + \eta_i^3 + 2\eta_i \sum_{j\neq i}^P \eta_j^2 \right) + 2\varepsilon \eta_i \Phi - \kappa_i \nabla^2 \eta_i \right),\ i=1,\ 2,\ \cdots,\ Q. \tag{4}$$

where L_i are kinetic coefficients related to grain boundary mobility with the units $m^3/(N\cdot s)$ and κ_i are gradient energy coefficients with the units J/m. m and ε are positive constants. A spatially dependent order parameter, $\Phi(\mathbf{r})$, is introduced to represent the dispersion of pores. The parameter assumes the value of 1 at the pore and becomes 0 in the matrix [16]. It is assumed that the pore dispersion is constant in time. We refer to Ref. [16] for a complete description of the model.

We applied the forward-Euler discretization scheme to discretize the time derivative of Eq. (4), as follows:

$$\eta_i(t+\Delta t) = \eta_i(t) + \frac{d\eta_i}{dt}\Delta t + O(\Delta t). \tag{5}$$

In our simulations, the phenomenological parameters in Eqs. (2)–(4) were set to $m = 1.0$, $\varepsilon = 1.0$ and $L_i = \kappa_i = 1.0$ for all i, by assuming an isotropic grain boundary mobility and grain boundary energy. We set $\Delta t = 0.1$ in Eq. (5) and $\Delta x = 1.0$ for calculating the Laplacian in Eq. (4). A periodic boundary condition was applied to all boundaries, was set to 1.0, and OpenMP parallelization was applied to efficiently utilize multicore CPU capability [17].

2.2. Steady-state thermal conduction analysis

In this study, heat conduction simulations based on the finite difference method were performed to calculate the thermal conductivity of polycrystalline UO_2 containing pores. In two dimensions, we simulated a square domain of measuring 20.48 μm × 20.48 μm, which was uniformly discretized into a 2048 × 2048 grid. Similarly, a cubic domain of length 2.56 μm in each direction, corresponding to a system with 256 × 256 × 256 grids, was simulated as a 3D system. The Dirichlet boundary condition with respect to a temperature of $T = 800\ K$ was applied at the edge of $x = 0$, and the Neumann boundary condition of $j = 50\ MW/m^2$ was applied at the edge of $x = 20.48$ μm (2.56 μm for three dimensions) to represent a constant heat flux flow along the x-direction. The values of T and j are arbitrarily selected and have no effect on the value of the calculated thermal conductivity. Adiabatic boundary conditions were enforced in the y- and z-directions. The temperature profile of the system was obtained by solving the steady-state conduction equation

$$\nabla k(r) \nabla T(r) = 0 \tag{6}$$

where $k(r)$ is the thermal conductivity, which varies with location depending on the underlying microstructure.

The effective thermal conductivity can be evaluated based on the rearranged Fourier's law as follows:

$$k_{eff} = \frac{j \times L_x}{\Delta T} \tag{7}$$

where L_x is the width of the domain, and ΔT is the average temperature drop across the simulation domain in the x-direction.

The steady-state heat conduction equation was solved using a finite-difference approximation based on the Crank–Nicolson (CN) implicit scheme and alternating direction implicit (ADI) methods. The CN method is unconditionally stable and second-order accurate in both time and space. The ADI method was employed to dimensionally decouple the heat equation for an efficient calculation using parallelization. We adopted CUDA GPU-parallelization and solved thousands of heat conduction equations simultaneously. A full description of the method is available in Ref. [10].

2.3. Microstructure and thermal conductivity dependence on local temperature

We used the summation of the phase-field order parameter η_i squared to represent the microstructure [18]. The grain boundary region indicated reduced values of less than 1 to incorporate the Kapitza resistance effect into the simulation. The value was 1 within the matrix and 0 inside the pore. Within the interface between different types of regions, the transition from one region to another was continuous. We assumed that the pores contained helium and set the lower bound of conductivity to $0.152 W/(K\cdot m)$, which corresponds to the thermal conductivity of helium gas. Although pores in irradiated UO_2 fuel are primarily filled with Xe, we used He as model fission gas, since low thermal conductivity of Xe can potentially cause a computational instability of simulation. The thermal conductivity dependent on the temperature and microstructure was determined using the parameter as follows [19]:

$$k(r) = \left(\sum_{i=1}^P \eta_i^2 \right)^{7.7} \times \left(k_{crystal} - 0.152 \right) + 0.152 \tag{8}$$

where 7.7 is the fitted value corresponding to approximately $10 MW/(m^2\cdot K)$ of the Kapitza conductance of the grain boundaries.

The lattice (crystal) thermal conductivity of pure UO_2 crystal based on only temperature was obtained from the model suggested by Harding and Martin [20]. It depends on temperature and is expressed in units of $W/(K\cdot m)$, as follows:

$$k_{crystal} = \frac{1}{0.0375 + 2.165 \times 10^{-4} T} + \frac{4.715 \times 10^9}{T^2} exp\left(\frac{-16361}{T} \right) \tag{9}$$

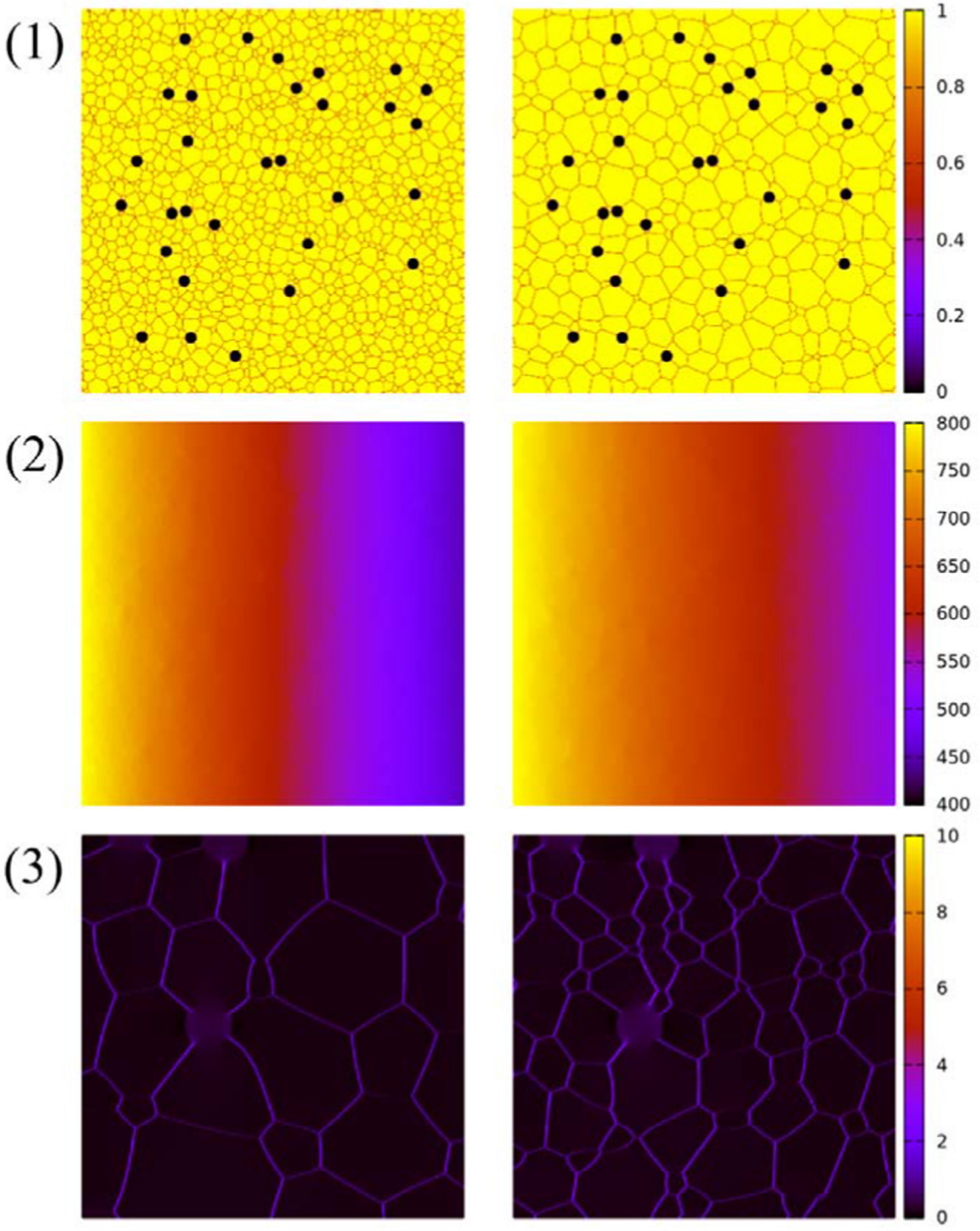

Fig. 1. Results obtained by 2D simulations of porosity = 2% and pore radii = 300 nm. (1) Microstructure represented using summation of phase-field order parameter η_i squared at (left) $d = 600$ nm and (right) $d = 1200$ nm. (2) Temperature distribution at steady-state in units of K (3) $|\nabla T(x,y)|$ at steady state.

3. Results and discussion

In a previous study [10], we investigated the effects of porosity and pore radius on the thermal conductivity of UO_2 single crystals and discovered that micrometer-scale pores can significantly affect thermal conduction. In this study, we conducted thermal analysis in the presence of grain boundaries and pores to investigate a more realistic UO_2 fuel. We employed the phase-field model of Moelans et al. [16] to generate the microstructures of UO_2 fuel. This model imparts a local pinning effect on grain boundary migration which leads to formation of intergranular gas bubbles aligned along grain boundaries. The details of the phase-field model and thermal analysis are described in Section 2. The combined effect of grain boundaries and intergranular pores on the effective thermal

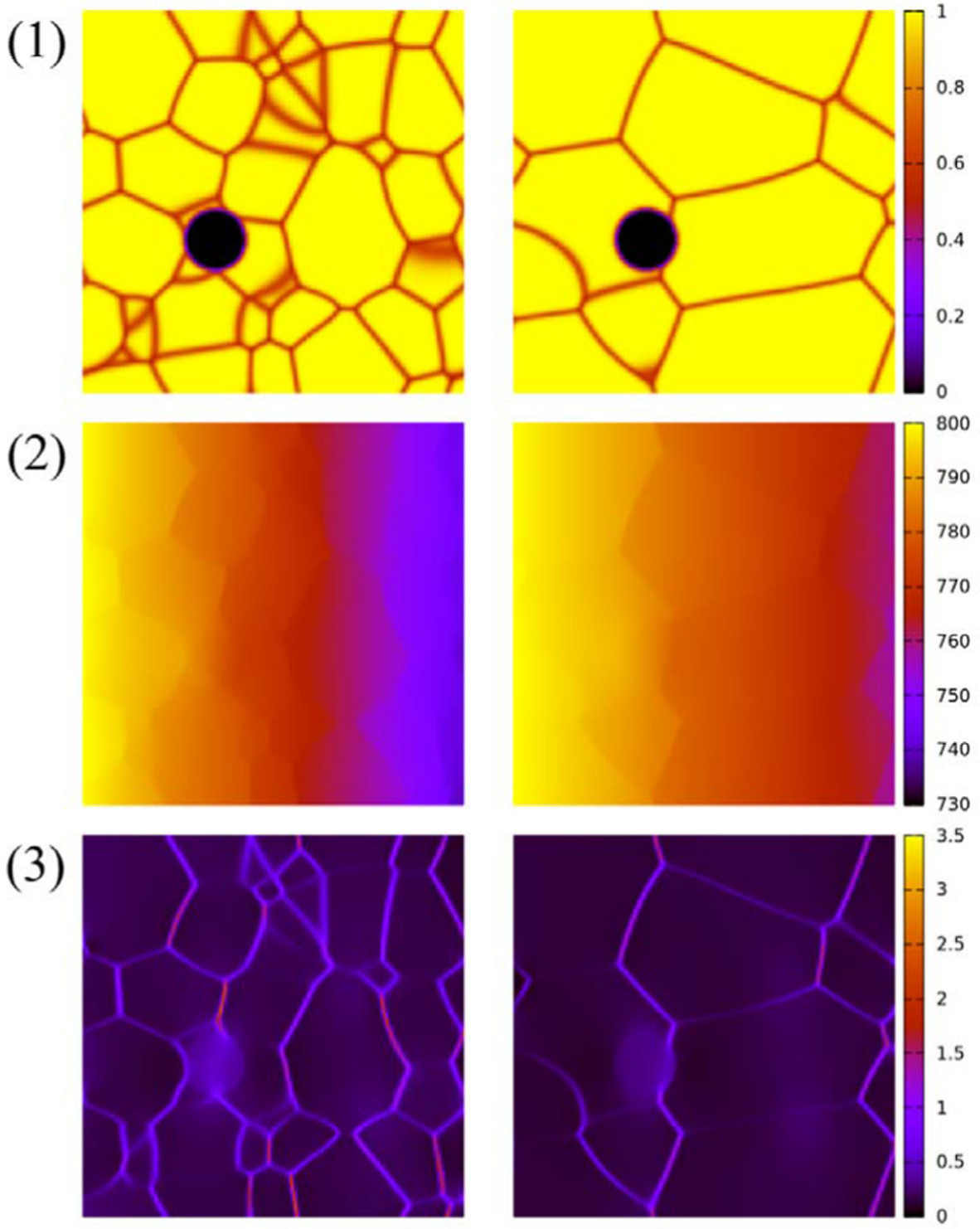

Fig. 2. Results obtained by 3D simulations of porosity = 2% and pore radii = 300 nm (cross section of $z = 5.12$ μm). (1) Microstructure represented using summation of phase-field order parameter η_i squared at (left) $d = 600$ nm and (right) $d = 1200$ nm. (2) Temperature distribution at steady-state in units of K (3) $|\nabla T(x, y, z)|$ at steady state.

conductivity was evaluated by systematically varying the porosity, pore size, and grain size. We analyzed systems with porosities of 0.01, 0.02, 0.03, and 0.04, for both 2D and 3D cases. Porosity was evaluated using the ratio of the number of grids occupied by the pores with respect to the total number of grids. In the 2D system, four different grain diameters ($d = 600$, 800, 1000, and 1200 nm) were considered. In the 3D system, two additional grain sizes ($d = 300$ and 400 nm) were considered for a more rigorous analysis. To quantify the pore radius effect on the effective conductivity in two and three dimensions, we measured the effective conductivity with different pore radii at specified porosities and grain sizes. Three different pore radii ($r = 100$, 200, and 300 nm) were analyzed

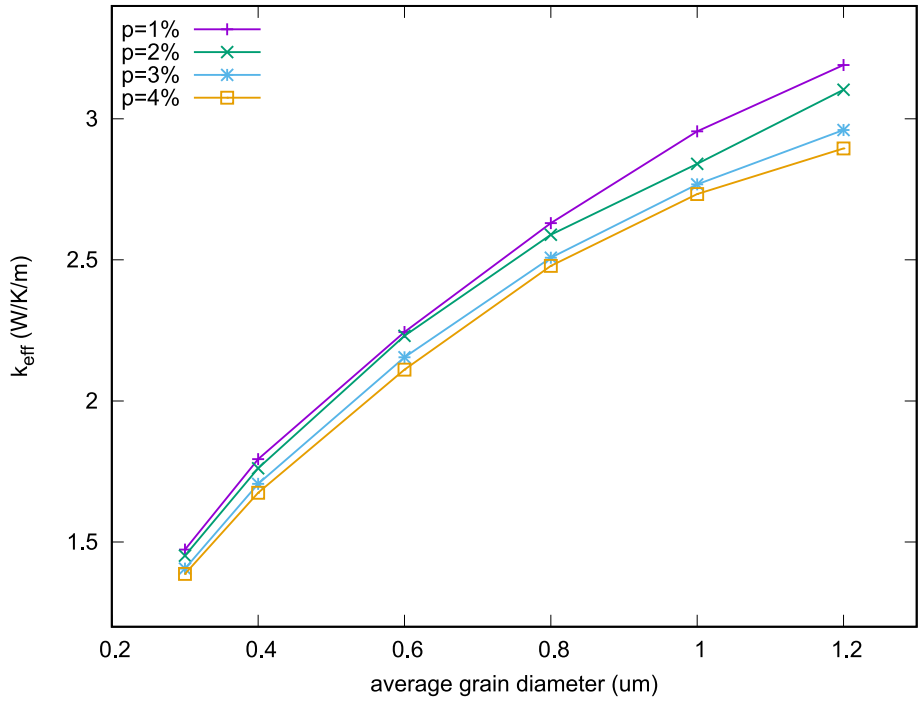

Fig. 3. Effective thermal conductivity obtained by 3D simulations of $r = 300$ nm with varying grain sizes and porosities.

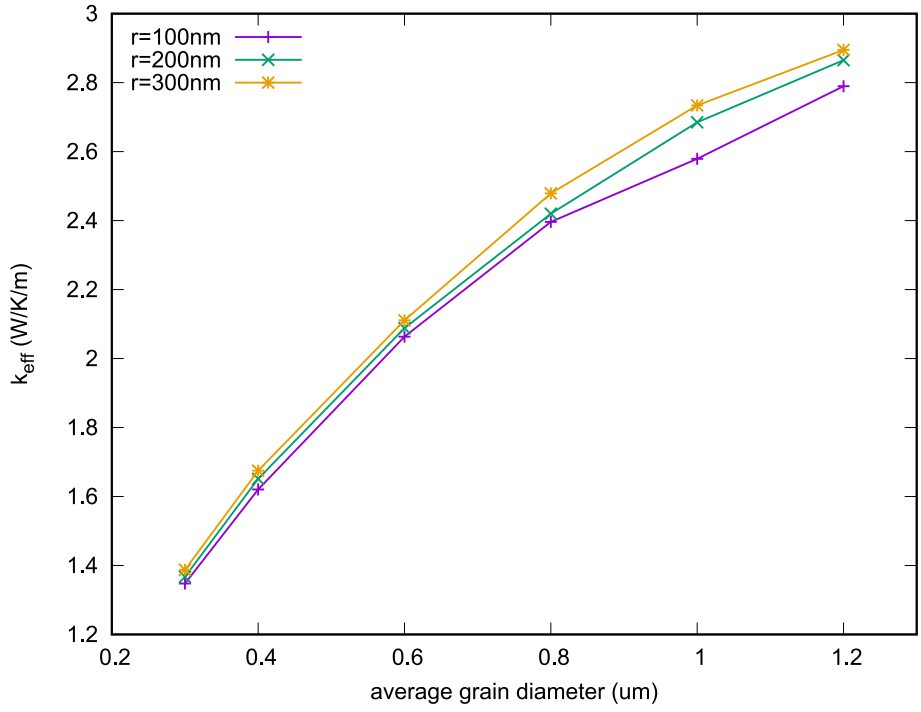

Fig. 4. Effective thermal conductivity obtained by 3D simulations of porosity = 4% with varying grain sizes and pore radii.

in both 2D and 3D systems. To simplify the situation, we assumed that all pores were circular in two dimensions and spherical in three dimensions, and that their radii were homogeneous for each set of simulations. We performed three sets of thermal conductivity simulations for each condition and averaged the effective conductivity to obtain more reliable results. Three sets of simulational microstructure were generated from the phase-field simulations which initially assigned randomly distributed pores of uniform size. The typical microstructures and their temperature profiles in the steady state are shown in Figs. 1 and 2. It was observed that monosized intergranular pores embedded in random positions without overlapping with each other. The temperature gradient was the highest in the grain boundary region, followed by the pore region and matrix region. As expected, the thermal conductivity

Table 1
The fitted value of exponent β in multiplier model of effective thermal conductivity at three different pore radii. The pores are circular in 2D and spherical in 3D microstructures.

The value of exponent β in multiplier model Eq. (10)		
	2D	3D
r = 100 nm	2.46884	2.41845
r = 200 nm	1.20273	1.88383
r = 300 nm	0.77723	1.66590

Table 2
Formulation of three effective thermal conductivity models of UO_2.

The effective thermal conductivity models of UO_2	
Model 1	$ln\left[\frac{k_{eff} \times (1 + k_0/G_k d)}{k_0}\right] = \beta \times \ln(1-p)$
Model 2	$ln\left[\frac{k_{eff} \times (1 + k_0/G_k d)}{k_0}\right] = \beta \times \ln(1-p)^n$
Model 3	$ln\left[\frac{k_{eff} \times (1 + k_0/G_k d)}{k_0}\right] = \beta \times \ln(1-p)^n + \alpha(1-p)$

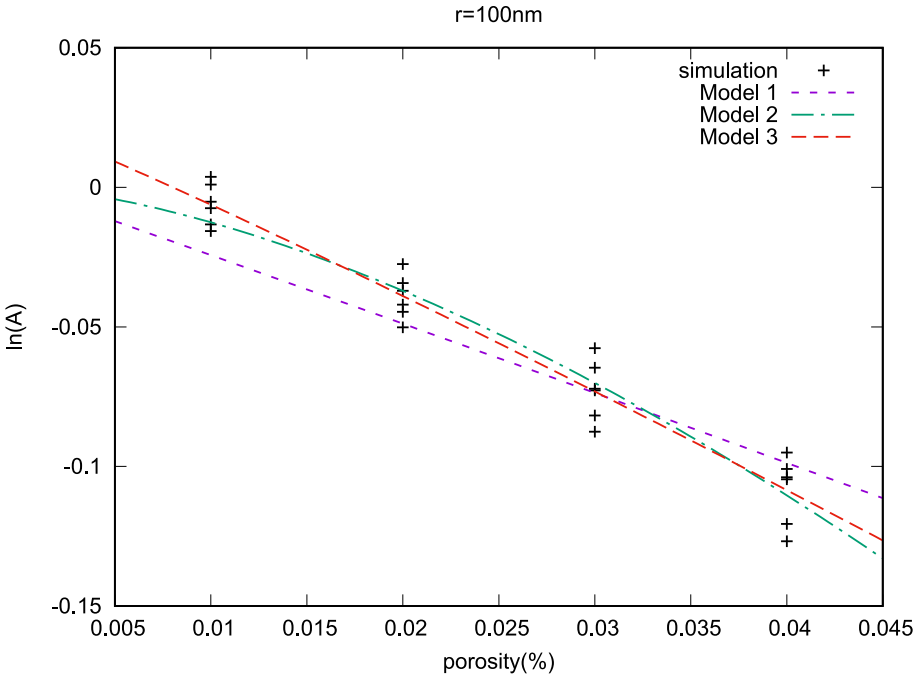

Fig. 5. Comparison between three models (lines) and simulation results (dots) at $r = 100$ nm in 3D simulations.

Table 3
Root mean square deviation values between obtained values from simulations and three fitted curves using Models 1, 2 and 3 for 2D system.

Root mean square deviations of 2D system			
Pore radius	Model 1	Model 2	Model 3
100 nm	0.0560	0.0381	0.0339
200 nm	0.0471	0.0349	0.0331
300 nm	0.0598	0.0509	0.0507

decreased as the porosity and grain diameter increased, as depicted in Fig. 3; this phenomenon is attributable to the lower thermal conductivity of the pore and grain boundary regions. Furthermore, we discovered that under a specified porosity and grain size, the thermal conductivity decreased with the pore radius, as shown in Fig. 4. The most widely used effective thermal conductivity model for porous polycrystal materials is the multiplier model [19], which multiplies the separate effect of porosity [13] and grain size [21] (Model 1), as follows:

Table 4
Root mean square deviation values between obtained values from simulations and three fitted curves using Models 1, 2 and 3 for 3D system.

Root mean square deviations of 3D system			
Pore radius	Model 1	Model 2	Model 3
100 nm	0.0341	0.0235	0.0217
200 nm	0.0355	0.0179	0.0157
300 nm	0.0334	0.0249	0.0209

$$k_{eff} = k_{eff}^{pore} \times k_{eff}^{GB} = k_0 \frac{(1-p)^{\beta}}{1 + k_0/(G_k d)} \tag{10}$$

where k_0 is the bulk conductivity of UO_2, G_k the Kapitza conductance, d the average grain diameter, p the porosity, and β the fitted value.

As shown in Table 1, the value of exponent β in Eq. (10) increases as the pore size decreases at a given porosity, which is consistent with the result of our previous study [10]. This indicates that a small pore-sized structure has a stronger influence on the effective conductivity than a large pore-sized structure.

However, our simulation results were not consistent with the multiplier model; therefore, we modified the formula to obtain a better fit. In Table 2, Model 1 is the multiplier model rearranged for β fitting. Model 2 is a modified equation, whose logarithmic term is a power function. We discovered that Model 2 slightly underestimated the thermal conductivity in the low-porosity regime; therefore, we modified the equation, as realized in Model 3. The right-hand sides of the equations in Table 2 were plotted against the porosity volume fraction, as shown in Fig. 5. Model 3 indicated the best fit among the three models.

To compare the accuracy of the three models, we evaluated the root-mean-square deviation (RMSD) of the models for each set of data obtained from simulations. The RMSD is the quadratic mean of the differences between values predicted by a model and the values observed, and it represents the magnitude of the prediction error for the dataset.

$$RMSD = \sqrt{\frac{1}{N}\sum^{N} |k_{simulation} - k_{model}|^2} \tag{11}$$

where $k_{simulation}$ is the effective conductivity value obtained from the simulation; k_{model} is the effective conductivity value predicted by Models 1, 2, and 3; N is the number of effective conductivity values compared.

Tables 3 and 4 show the RMSD values of the three models at particular grain diameters in two and three dimensions. Model 3 indicated the lowest RMSD for both two and three dimensions.

4. Conclusions

In the mesoscale regime, we computationally investigated the effects of porosity, pore size, and grain boundaries on the effective conductivity of porous polycrystalline UO_2 in 2D and 3D systems. The effective conductivities were effectively estimated using the CN and ADI methods via the implementation of CUDA GPU parallelization. We evaluated the exponent value β of the multiplier model of effective thermal conductivity for both 2D and 3D cases at different circular (2D) and spherical (3D) pore radii, and we found that exponent β decreases as the pore radius increases. We proposed modified multiplier models for the effective conductivity of porous polycrystal UO_2 based on the microstructure generated using the phase-field method in the presence of pores. This empirical model has an excellent predictive power in the range of our simulation. However, significant work is still needed to develop a physically based model of effective conductivity without using fitting parameters.

Declaration of competing interest

The authors declare that they have no known competing financial interests or personal relationships that could have appeared to influence the work reported in this paper.

Acknowledgments

This work was supported by a National Research Foundation of Korea (NRF) grant funded by the Korean government (MSIT) (NRF-2017M2B2B1072806). This work was also supported by the “Human Resources Program in Energy Technology” of the Korea Institute of Energy Technology Evaluation and Planning (KETEP), granted financial resources from the Ministry of Trade, Industry Energy, Republic of Korea (No. 20214000000070).

References

[1] Kenneth Geelhood, Walter G. Luscher, Patrick A. Raynaud, Ian E. Porter, FRAPCON-4.0: A Computer Code for the Calculation of Steady-State Thermal-Mechanical Behavior of Oxide Fuel Rods for High Burn-Up, vol. 1, Pacific Northwest National Laboratory-19418, Richland, Washington, 2015.
[2] P.G. Lucuta, Hj Matzke, I.J. Hastings, A pragmatic approach to modelling thermal conductivity of irradiated UO_2 fuel: review and recommendations, J. Nucl. Mater. 232 (1996) 166–180.
[3] Michael R. Tonks, Xiang-Yang Liu, David Andersson, Danielle Perez, Aleksandr Chernatynskiy, Giovanni Pastore, Christopher R. Stanek, Richard Williamson, Development of a multiscale thermal conductivity model for fission gas in UO_2, J. Nucl. Mater. 469 (2016) 89–98.
[4] Tianyi Chen, Di Chen, Bulent H. Sencer, Lin Shao, Molecular dynamics simulations of grain boundary thermal resistance in UO_2, J. Nucl. Mater. 452 (2014) 364–369.
[5] C.-W. Lee, Aleksandr Chernatynskiy, Priyank Shukla, R.E. Stoller, Susan B. Sinnott, Simon Robert Phillpot, Effect of pores and He bubbles on the thermal transport properties of UO_2 by molecular dynamics simulation, J. Nucl. Mater. 456 (2015) 253–259.
[6] Weiming Chen, Michael W.D. Cooper, Ziqi Xiao, David A. Andersson, Xian-Ming Bai, Effect of Xe bubble size and pressure on the thermal conductivity of UO_2—a molecular dynamics study, J. Mater. Res. 34 (2019) 2295–2305.
[7] Paul C. Millett, Michael R. Tonks, Meso-scale modeling of the influence of intergranular gas bubbles on effective thermal conductivity, J. Nucl. Mater. 412 (2011) 281–286.
[8] Paul C. Millett, Michael R. Tonks, K. Chockalingam, Yongfeng Zhang, S.B. Biner, Three dimensional calculations of the effective Kapitza resistance of UO_2 grain boundaries containing intergranular bubbles, J. Nucl. Mater. 439 (2013) 117–122.
[9] Linyun Liang, Yeon Soo Kim, Zhi-Gang Mei, Larry K. Aagesen, Abdellatif M. Yacout, Fission gas bubbles and recrystallization-induced degradation of the effective thermal conductivity in U-7Mo fuels, J. Nucl. Mater. 511 (2018) 438–445.
[10] Bohyun Yoon, Kunok Chang, Effect of the pore radius on the effective conductivity of UO_2 in 2D and 3D: a computational approach, Results in physics 19 (2020) 103440.
[11] D.R. Olander, Fundamental Aspects of Nuclear Reactor Fuel Elements, U.S. Energy Research and Development Administration, Dept. of energy, National technical information service, springfield, VA, 1976.
[12] S.K. Rhee, Porosity—thermal conductivity correlations for ceramic materials, Mater. Sci. Eng. 20 (1975) 89–93.
[13] G. Ondracek, B. Schulz, The porosity dependence of the thermal conductivity for nuclear fuels, J. Nucl. Mater. 46 (1973) 253–258.
[14] Long-Qing Chen, Wei Yang, Computer simulation of the domain dynamics of a quenched system with a large number of nonconserved order parameters: the

grain-growth kinetics, Phys. Rev. B 50 (1994) 15752.
[15] Srikanth Vedantam, B.S.V. Patnaik, Efficient numerical algorithm for multi-phase field simulations, Phys. Rev. 73 (2006), 016703.
[16] Nele Moelans, Bart Blanpain, Patrick Wollants, A phase field model for the simulation of grain growth in materials containing finely dispersed incoherent second-phase particles, Acta Mater. 53 (2005) 1771–1781.
[17] L. Dagum, R. Menon, OpenMP: an industry standard API for shared-memory programming, IEEE Comput. Sci. Eng. 5 (1998) 46–55.
[18] D. Fan, L.-Q. Chen, Computer simulation of grain growth using a continuum field model, Acta Mater. 45 (1997) 611–622.
[19] Paul C. Millett, Dieter Wolf, Tapan Desai, Srujan Rokkam, Anter El-Azab, Phase-field simulation of thermal conductivity in porous polycrystalline microstructures, J. Appl. Phys. 104 (2008), 033512.
[20] J.H. Harding, D.G. Martin, A recommendation for the thermal conductivity of UO_2, J. Nucl. Mater. 166 (1989) 223–226.
[21] Ho-Soon Yang, G.-R. Bai, L.J. Thompson, Jeffrey A. Eastman, Interfacial thermal resistance in nanocrystalline yttria-stabilized zirconia, Acta Mater. 50 (2002) 2309–2317.